# A GENERIC DEMOSAICING ALGORITHM BASED ON A DIFFUSION MODEL

*Alain Horé, Djemel Ziou, and Marie-Flavie Auclair-Fortier*

MOIVRE, Department of Computer Science, University of Sherbrooke
2500, Boulevard de l'Université, Sherbrooke (Qc), J1H 2R1, Canada

## ABSTRACT

In this paper, a diffusion-based generic demosaicing algorithm is proposed which can be used for various sensor images captured by digital cameras equipped with various RGB color filter arrays. This algorithm improves our previous edge-sensing generic demosaicing algorithm by enhancing the computation of the green band. In fact, since the green band plays a major and crucial role in the performance of the edge-sensing generic demosaicing algorithm, a diffusion-based model is used for reducing the errors generated when computing the green band. A series of tests has been made on images of the Kodak database, and our diffusion-based demosaicing algorithm performs better than the edge-sensing generic demosaicing algorithm in regard to both subjective and objective evaluation.

***Index Terms***— Demosaicing, diffusion, inverse diffusivity, color filter array, spectral interpolation.

## 1. INTRODUCTION

A full-color image is usually composed of three color planes and, accordingly, three separate sensors are required for a camera to measure an image. To reduce the cost, many cameras use a single sensor covered with a color filter array (CFA). The CFA consists of a set of spectrally selective filters that are arranged in an interleaved pattern so that each sensor pixel samples one of three primary color components. These sparsely sampled color values are termed mosaiced images. To render a full-color image from a mosaiced image, an image reconstruction process, commonly known as CFA interpolation or CFA demosaicing [1], is required to estimate for each multispectral pixel its two missing color values. Many demosaicing algorithms have been proposed over the last decade [2]. They play a major role in the demosaicing process, as summarized in Fig. 1, in order to obtain a final image close to the original image. Mathematically, given a mosaiced image $g$ and a CFA pattern $m$, all of size $M \times N$ and such that $g(i, j)$ and $m(i, j)$ are 3-components vectors of red, green and blue color values, the demosaicing problem consists in finding an image $h$ such that $g(i, j)_k = h(i, j)_k \times m(i, j)_k$ for $k \in \{1, 2, 3\}$ and $m(i, j) \in \{[1, 0, 0], [0, 1, 0], [0, 0, 1]\}$, with the image $h$ being as close as possible to the original image $f$ with respect to visual assessment or objective quality measures. In [7], Lukac *et al.* have proposed an interesting universal demosaicing algorithm which can be used for various CFA patterns based on RGB colors. Even if that algorithm generally performs well, it exhibits some artefacts (zipper effect, color aliasing) around edges. In [8], we have proposed a generic demosaicing algorithm that improves the algorithm of Lukac *et al.* by embedding an edge detection model as well as properly modifying the color difference model used for the spectral interpolation. Our algorithm greatly depends on the initial computation of the green band, which impacts the overall quality of the demosaiced images. In this paper, we improve the computation of the green band by using a diffusion model which enhances the anisotropic diffusion equation in the case of image demosaicing [9]. The model that we propose re-

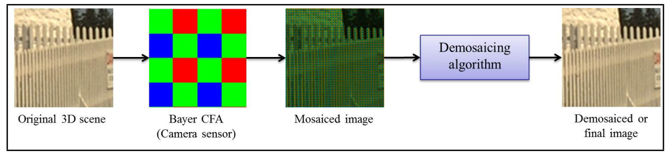


**Fig. 1**: The demosaicing process.

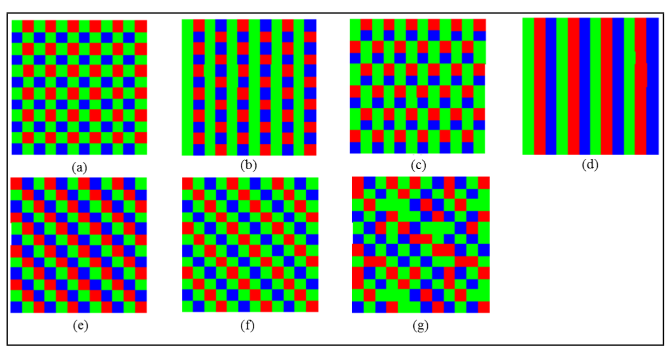


**Fig. 2**: Some RGB CFAs: (a) Bayer CFA [3]. (b) Yamanaka CFA [4]. (c) Lukac *et al.* CFA [5]. (d) Vertical stripe CFA. (e) Diagonal stripe CFA. (f) Modified Bayer CFA. (g) HVS-based CFA [6].

A. Horé, D. Ziou, and M. F. Auclair-Fortier are with the MOIVRE, Department of Computer Science, University of Sherbrooke, Sherbrooke (Québec), J1K2R1, Canada. Email: {alain.hore,djemel.ziou,marie-flavie.auclair-fortier}@usherbrooke.ca.

duces the reconstruction error of the green band, which also contributes in reducing the overall reconstruction error of the demosaiced images.

The rest of the paper is organized as follows: in Section 2, we revisit our initial generic demosaicing algorithm; in Section 3, we introduce the diffusion model for improving the generic demosaicing algorithm; in Section 4, we present some experimental results, and we end the paper with the concluding remarks.

## 2. THE GENERIC DEMOSAICING ALGORITHM

Due to the monochromatic nature of the sensor, the captured values from a CFA pattern create an $M \times N$ image $F : \mathbb{N}^2 \rightarrow \mathbb{N}$. This CFA image represents a two-dimensional matrix of integer samples $F(p,q)$ with $p = 1, 2, ..., M$ and $q = 1, 2, ..., N$ denoting the image rows and columns, respectively. The demosaicing step re-arranges the acquired sensor data to an RGB-like vectorial field, and completes missing color components using adjacent sensor data through spectral interpolation. The process produces a color image $I : \mathbb{N}^2 \rightarrow \mathbb{N}^3$ with color pixels $I(p,q) = [I(p,q)_1, I(p,q)_2, I(p,q)_3]$ represented as vectors in the RGB vectorial space. $I(p,q)_1$ represents the red (R) component, $I(p,q)_2$ the green (G) component, and $I(p,q)_3$ the blue (B) component. Also, a $M \times N$ vectorial field $d : \mathbb{N}^2 \rightarrow \{0,1\}^3$ of the corresponding location flags is initialized using the default value $d(p,q)_k = 1$ to indicate that the primary color indexed by $k$ is found in the CFA at position $(p,q)$. In the CFA shown in Fig. 3 for example, we have $d(p,q)_1 = 0$, $d(p,q)_2 = 1$, $d(p,q)_3 = 0$. After initialization, the algorithm follows some conventional practices [10], and starts by estimating the missing green components through a weighted sum-based interpolation controlled by an edge-detection algorithm. Then, the red and blue components are estimated from the green components by using a constant color-difference model. Finally, a post-processing step is applied on the green components and then on the red and blue components to improve the image quality.

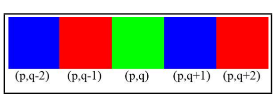


**Fig. 3**: Part of a CFA pattern.

## 3. IMPROVEMENT OF THE GENERIC DEMOSAICING ALGORITHM

The generic demosaicing algorithm is highly dependent on the quality of the initial reconstruction of the green color band. Consequently, a poor reconstruction of the green color band will have a disastrous impact on the reconstruction of the red and blue color bands. In this section, we improve the computation of the green band by using a diffusion model. For this purpose, we will consider that the interpolation of the green color band given by the original generic demosaicing algorithm is a starting point of a diffusion process that improves the quality of the color band recursively. In fact, by using a diffusion model, we will be able to perform edge-preserving smoothing while also preserving the fidelity to the original lower-resolution image (in fact, the CFA/mosaiced image is considered here as a low-resolution image). In some previous works, diffusion has been used as a post-processing step of demosaicing algorithms in order to enhance the quality of images [11, 12].

Diffusion is analytically defined using the following partial differential equation (PDE):

$$\begin{cases} \frac{\partial f(x,y,t)}{\partial t} = \operatorname{div}\left[\lambda(x,y,t)\nabla f(x,y,t)\right] \\ f(x,y,0) = f_0(x,y) \end{cases} \quad (1)$$

where $f(x,y,t)$ is the image at pixel location $(x,y)$ and time $t$, $\lambda(x,y,t)$ the diffusion coefficient for image $f$ at location $(x,y)$ and time $t$, div the divergence operator, and $\nabla$ the gradient operator. At the initial time $t = 0$, $f$ is equal to $f_0$, which is the starting point of the diffusion process. This starting point, in the case of image demosaicing, can be any approximation of the demosaiced image, which can be obtained by using for example the Bilinear demosaicing algorithm or any existing image demosaicing algorithm. The expression used for $\lambda$ in this paper is:

$$\lambda(x,y,t) = \frac{1}{1 + \left(\frac{\|\nabla f(x,y,t)\|}{\beta}\right)^2} \quad (2)$$

In Eq. (2), the coefficient $\beta$ controls the diffusion factor, and $\lambda$ is a decreasing function of the magnitude of the gradient. We note that $0 < \lambda(x,y,t) \leq 1$. The PDE given in Eq. (1) is efficient for blurring and reducing noise, but it is not efficient for reducing edge artefacts such as aliasing and zipper effect that may be found in demosaicing algorithms [9, 13]. In this paper, we revisit that diffusion model and we improve it in order to enhance image demosaicing. By decomposing the divergence operator, Eq. (1) is equivalent to:

$$\begin{cases} \frac{\partial f(x,y,t)}{\partial t} = \lambda(x,y,t)\Delta f(x,y,t) + \nabla\lambda(x,y,t) \times \nabla f(x,y,t) \\ f(x,y,0) = f_0(x,y) \end{cases} \quad (3)$$

where $\times$ denotes the scalar product, and $\Delta$ the Laplacian operator. We will now show that PDE (3) is not suitable for reducing edge artefacts found in image demosaicing. In [14], it is shown that:

$$\Delta f(x,y,t) = \frac{\partial^2 f(x,y,t)}{\partial n^2} + \frac{\partial^2 f(x,y,t)}{\partial n_\perp^2} = \frac{\partial^2 f(x,y,t)}{\partial n^2} + \kappa(x,y,t)\,\|\nabla\lambda(x,y,t)\| \quad (4)$$

where $n$ is the direction of the gradient, $n_\perp$ the normal direction of the gradient, $\kappa$ the local curvature, which is given by (in practice, 1 is added to the denominator to avoid null values which can occur in constant regions for example):

$$\kappa = \frac{f_x^2 f_{yy} - 2 f_x f_y f_{xy} + f_y^2 f_{xx}}{\left(f_x^2 + f_y^2\right)^{3/2}} \quad (5)$$

where $f_x$ (resp. $f_y$) is the first order derivative of $f$ along $x$ (resp. $y$), $f_{xx}$ (resp. $f_{yy}$) is the second order derivative of $f$ along $x$ (resp. $y$), $f_{xy}$ is the mixed derivative of $f$ along $x$ and $y$. By rewritting the scalar product $\nabla\lambda(x,y,t) \times \nabla f(x,y,t)$, PDE (3) then becomes:

$$\begin{cases} \frac{\partial f(x,y,t)}{\partial t} & = \lambda(x,y,t)\frac{\partial^2 f(x,y,t)}{\partial n^2} + [\lambda(x,y,t)\kappa + \\ & \|\nabla\lambda(x,y,t)\| \cos\phi(x,y,t)] \, \|\nabla f(x,y,t)\| \\ f(x,y,0) = f_0(x,y) \end{cases} \tag{6}$$

where $\phi(x,y,t)$ denotes the angle between $\nabla\lambda(x,y,t)$ and $\nabla f(x,y,t)$. PDE (6) contains two interesting terms: the first right term corresponds to the diffusion of the image luminance in the gradient direction, and it is related to the normal curvature $K_n$ along the gradient direction. The second term in PDE (6) is related to the diffusion of the image luminance along the direction orthogonal to the gradient, which corresponds to the direction of potential edges. Thus, this is normally the main part of the diffusion equation that plays a major role in reducing edge artefacts such as aliasing or zipper effect. Consequently, we will reduce PDE (6) to the terms that are meaningful for reducing edge artefacts:

$$\begin{cases} \frac{\partial f(x,y,t)}{\partial t} = [\lambda(x,y,t)\kappa + \|\nabla\lambda(x,y,t)\| \cos\phi(x,y,t)] \, \|\nabla f(x,y,t)\| \\ f(x,y,0) = f_0(x,y) \end{cases} \tag{7}$$

Let us focus now on the diffusion process given by PDE (7). In the vicinity of a step edge, the magnitude of the gradient is high, and $\lambda(x,y,t)$ is small and approaches 0: thus, diffusion is weak and the reduction of edge artefacts (thanks to smoothing) is also weak (we assume that $\nabla\lambda(x,y,t)$ is also small since $\lambda(x,y,t)$ is small). In a homogeneous region, $\nabla f(x,y,t)$ approaches zero, and $\lambda(x,y,t)$ is high and approaches 1: consequently, a strong reduction of potential edge artefacts is carried out due to the smoothing imposed by diffusion. In fact, this behaviour is not suitable for reducing edge artefacts. Indeed, in the vicinity of an edge, we need a strong reduction of edge artefacts, while it is not needed in homogeneous regions since homogeneous regions do not generally exhibit edge artefacts or unpleasant visual artefacts. To solve that issue, we replace in PDE (7) the diffusivity term $\lambda(x,y,t)$ by the *inverse diffusivity* $1-\lambda(x,y,t)$. This is valid since $0 < \lambda(x,y,t) \leq 1$. Thus, the modified PDE (7) is:

$$\begin{cases} \frac{\partial f(x,y,t)}{\partial t} = [(1-\lambda(x,y,t))\,\kappa - \|\nabla\lambda(x,y,t)\| \cos\phi(x,y,t)] \, \|\nabla f(x,y,t)\| \\ f(x,y,0) = f_0(x,y) \end{cases} \tag{8}$$

We should note that we have obtained PDE (8) by also noticing the following property regarding the scalar product:

$$\nabla(1-\lambda(x,y,t)) \times \nabla f(x,y,t) = -\nabla\lambda(x,y,t) \times \nabla f(x,y,t) \tag{9}$$

The inverse diffusivity $1-\lambda(x,y,t)$ is an increasing function with respect to the magnitude of the gradient $\|\nabla f(x,y,t)\|$. Consequently, near edges, $\|\nabla f(x,y,t)\|$ is high and $1-\lambda(x,y,t)$ approaches 1. Thus, a strong diffusion is performed, which reduces edges artefacts. On the other hand, in homogeneous regions, $\|\nabla f(x,y,t)\|$ approaches 0 and $1-\lambda(x,y,t)$ also approaches 0. Consequently, diffusion is not performed or is negligible, which is desirable. To further simplify PDE (9), we have noticed through some experiments that the term $-\|\nabla\lambda(x,y,t)\| \cos\phi(x,y,t)$ is negligible compared to the term $(1-\lambda(x,y,t))\,\kappa$. Consequently, we will use the following PDE for improving image demosaicing through diffusion:

$$\begin{cases} \frac{\partial f(x,y,t)}{\partial t} = [1-\lambda(x,y,t)] \, \|\kappa(x,y,t)\nabla\lambda(x,y,t)\| \\ f(x,y,0) = f_0(x,y) \end{cases} \tag{10}$$

In practice, Eq. (10) can be applied for each band of the color space in which the image $f_0$ is represented. In this paper however, we apply the diffusion model given by Eq. (10) only to the green color band, which is represented by $f_0$. The term $f$ is then the enhanced green color band. We also note that, in practice, Eq. (10) is executed iteratively, and the image is thus iteratively improved until a maximal number of iterations is reached. For the iteration to take place, we make the approximation given by Eq. (11), where $\delta t$ can be seen as the iteration or time step ($\delta t = 0.15$ is used in this paper).

$$\frac{\partial f(x,y,t)}{\partial t} = \frac{f(x,y,t+\delta t) - f(x,y,t)}{\delta t} \tag{11}$$

However, by strictly applying Eq. (10) iteratively, all the values of the pixels in the image will be modified. This default behavior needs to be revised since there are locations where the green color value is exactly known from the mosaiced (or low-resolution) image (those for which $d(x,y)_2 = 1$, see Section 2). Thus, for taking into account that constraint of pixel locations where the value of the green color is known, we modify Eq. (10) as follows:

$$\begin{cases} \frac{\partial f(x,y,t)}{\partial t} = [1-\lambda(x,y,t)] \, \|\kappa(x,y,t)\nabla\lambda(x,y,t)\| \\ f(x,y,0) = f_0(x,y) \\ f(x,y,t) = f_0(x,y) \text{ if } d(x,y)_2 = 1 \end{cases} \tag{12}$$

## 4. EXPERIMENTAL RESULTS

In this section, we use a set of 15 images of the Kodak database [15] for comparing our original generic demosaicing algorithm [8] with the improved algorithm proposed in this paper. The final image corresponding to each demosaicing algorithm is compared to the original image for quality measurement through the color mean square error (MSE). A smaller value of MSE indicates smaller reconstruction errors. In our experiment, we note that the size of the interpolation window placed at the center of each pixel is set to 5, and the number of iterations used for the diffusion process is 4. The diffusivity term of the diffusion process is given by Eq. (2) with $\beta = 1$. In Fig. 4, we present a part of an original image as well as the images obtained through the two demosaicing algorithms in comparison for the CFA shown in Fig. 2c. As we can notice, the original demosaicing algorithm produces more color aliasing and visual artefacts than the diffusion-based demosaicing algorithm. Thus, by improving the computation of the green band through a diffusion process, we have improved the quality of the demosaiced image, and this

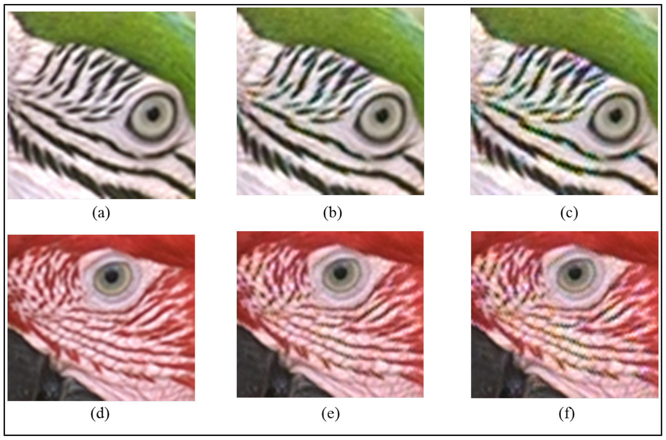


**Fig. 4**: (a) and (d) Parts of an original image. (b) and (e) Images obtained using our diffusion-based generic demosaicing algorithm with the CFA pattern shown in Fig. 2c ($MSE = 10.51$). (c) and (f) Images obtained using the original generic demosaicing algorithm [8] with the same CFA pattern ($MSE = 13.56$).

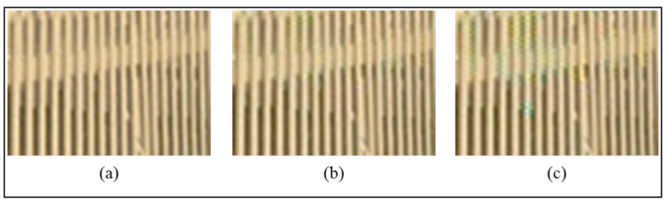


**Fig. 5**: (a) Part of an original image. (b) Image obtained using our improved generic demosaicing algorithm with the CFA pattern shown in Fig. 2c ($MSE = 34.57$). (c) Image obtained using the original generic demosaicing algorithm [8] with the same CFA pattern ($MSE = 38.59$).

confirms the impact of the green band on the overall quality of the demosaicing as was presented in Section 3. In Fig. 5, we notice again the improvement of the quality of the images obtained with the diffusion-based demosaicing algorithm compared to the original generic demosaicing algorithm. In Table 1 we present the difference between the MSE values of the original generic demosaicing algorithm and the MSE values of the improved generic demosaicing algorithm. As can be observed in Table 1, all the differences of the MSE values between the improved demosaicing algorithm and the original generic demosaicing algorithm are positive. This means that the improved diffusion-based generic demosaicing algorithm do enhance the quality of the reconstruction of images when compared to the original generic demosaicing algorithm. This applies for all the CFA patterns used. Also, among all the CFA patterns used, we notice that the enhancement of the reconstruction of images by our diffusion-based generic demosaicing algorithm is stronger for the CFA c, while it is weaker for the TV pattern (CFA d). Thus, it appears that the different CFA patterns respond differently to the integration of our diffusion model to the generic demosaicing algorithm.

## 5. CONCLUSION

In this paper, we have proposed an enhancement of the edge-sensing generic demosaicing algorithm by using a diffusion-based model. The main purpose of the diffusion-based model is to improve the computation of the green band which plays a major role in the overall reconstruction of demosaiced images. Experimental results based on various images have confirmed the improvement of the quality of images with the diffusion-based model since images have less visual artefacts and smaller MSE values.

**Table 1**: $MSE_{Original} - MSE_{Improved}$ for the different images and for the different CFAs shown in Fig. 2.

| Image no | CFA a | CFA b | CFA c | CFA d | CFA e | CFA f | CFA g |
|---|---|---|---|---|---|---|---|
| a | 2.15 | 5.04 | 11.93 | 0.54 | 3.52 | 5.80 | 4.52 |
| b | 0.80 | 1.10 | 2.15 | 0.42 | 0.95 | 1.37 | 1.62 |
| c | 0.84 | 1.33 | 3.03 | 0.63 | 1.72 | 1.30 | 0.93 |
| d | 1.09 | 1.70 | 3.29 | 0.46 | 1.95 | 1.58 | 1.53 |
| e | 4.43 | 6.57 | 17.24 | 2.12 | 9.08 | 7.38 | 5.45 |
| f | 1.71 | 4.49 | 10.08 | 1.28 | 3.47 | 3.80 | 3.49 |
| g | 1.03 | 1.27 | 2.67 | 0.64 | 1.72 | 1.62 | 1.32 |
| h | 3.64 | 5.98 | 14.00 | 1.44 | 6.44 | 5.89 | 7.41 |
| i | 0.88 | 1.06 | 2.54 | 0.56 | 1.44 | 1.41 | 1.51 |
| j | 0.85 | 1.25 | 3.15 | 0.53 | 1.76 | 1.63 | 1.83 |
| k | 1.52 | 2.84 | 5.76 | 1.12 | 2.21 | 2.97 | 2.26 |
| l | 0.60 | 0.90 | 2.42 | 0.31 | 1.27 | 1.12 | 0.96 |
| m | 5.36 | 11.82 | 22.27 | 3.21 | 10.13 | 10.15 | 8.77 |
| n | 1.39 | 2.02 | 4.03 | 1.29 | 1.94 | 1.90 | 2.52 |
| o | 0.88 | 1.07 | 3.12 | 0.45 | 1.55 | 1.58 | 1.06 |
| **Average** | **1.81** | **3.23** | **7.18** | **1.00** | **3.28** | **3.30** | **3.01** |

## 6. REFERENCES


[1] C. Y. Tsai and K. Y. Song, “A new edge-adaptive demosaicing algorithm for color filter arrays,” *Image and Vision Computing*, vol. 25, no. 9, pp. 1495–1508, 2007.

[2] L. S. Lee, W. and J. Kim, “Cost-effective color filter array demosaicing using spatial correlation,” *IEEE Transactions on Consumer Electronics*, vol. 52, no. 2, pp. 547–554, 2006.

[3] B. E. Bayer, “Color imaging array,” *US patent 3971065*, 1976.

[4] S. Yamanaka, “Solid state camera,” *US patent 4054906*, 1977.

[5] R. Lukac and K. N. Plataniotis, “Color filter arrays: design and performance analysis,” *IEEE Transactions on Consumer Electronics*, vol. 51, no. 4, pp. 1260–1267, 2004.

[6] M. Parmar and S. J. Reeves, “A perceptually based design methodology for color filter arrays,” in *IEEE International Conference on Acoustics, Speech, and Signal Processing (ICASSP)*, vol. 3, 2004, pp. 473–476.

[7] R. Lukac and K. N. Plataniotis, “Universal demosaicking for imaging pipelines with an rgb color filter array,” *Pattern Recognition*, vol. 38, no. 11, pp. 2208–2212, 2005.

[8] A. Horé and D. Ziou, “An edge-sensing generic demosaicing algorithm with application to image resampling,” *IEEE Transactions on Image Processing*, vol. 20, no. 11, pp. 3136–3150, 2011.

[9] P. Perona and J. Malik, “Scale-space and edge detection using anisotropic diffusion,” *IEEE Transactions on Pattern Analysis and Machine Intelligence*, vol. 12, no. 7, pp. 629–639, 1990.

[10] B. K. Gunturk, J. Glotzbach, Y. Altunbasak, R. W. Schafer, and R. M. Mersereau, “Demosaicking: color filter array interpolation,” *IEEE Signal Processing Magazine*, vol. 22, no. 1, pp. 44–54, 2005.

[11] R. Kimmmel, “Demosaicing: image reconstruction from ccd samples,” *IEEE Transactions on Image Processing*, vol. 8, no. 9, pp. 1221–1228, 1999.

[12] J. Herwig and J. Pauli, “Regularized color demosaicing via luminance approximation,” in *European Conference on Colour in Graphics, Imaging, and Vision*, 2010, pp. 62–69.

[13] D. Ziou and A. Horé, “Reducing aliasing in images: a pde-based diffusion revisited,” *Pattern Recognition*, vol. 45, no. 3, pp. 1180–1194, 2012.

[14] J. J. Clark, “Authenticating edges produced by zero-crossing algorithms,” *IEEE Transactions on Pattern Analysis and Machine Intelligence*, vol. 11, no. 1, pp. 43–57, 1989.

[15] Kodak, “Kodak Lossless True Color Image Suite,” http://r0k.us/graphics/kodak/, 2012.